# Spray penetration, combustion, and soot formation characteristics of the ECN Spray C and Spray D injectors in multiple combustion facilities

Noud Maes, Scott A Skeen, Michele Bardi, Russell P Fitzgerald, Louis-Marie Malbec, Gilles Bruneaux, Lyle M Pickett, Koji Yasutomi, Glen Martin

Applied Thermal Engineering 172 (2020) 115136

Contents lists available at ScienceDirect

Applied Thermal Engineering

journal homepage: www.elsevier.com/locate/apthermeng

# Spray penetration, combustion, and soot formation characteristics of the ECN Spray C and Spray D injectors in multiple combustion facilities

Noud Maes[a,b,d,*], Scott A. Skeen[b,c], Michele Bardi[d], Russell P. Fitzgerald[f], Louis-Marie Malbec[d], Gilles Bruneaux[d], Lyle M. Pickett[b,*], Koji Yasutomi[b,f], Glen Martin[e]

[a] Department of Mechanical Engineering, Eindhoven University of Technology, P.O. Box 513, 5600 MB Eindhoven, the Netherlands
[b] Combustion Research Facility, Sandia National Laboratories, P.O. Box 969, MS 9053, Livermore, CA 94551, USA
[c] Department of Mechanical Engineering, Dixie State University, 225 S University Ave., St George, UT 84770, USA
[d] IFP Energies Nouvelles, 92852 Rueil-Malmaison Cedex, France; Institut Carnot IFPEN Transports Energie, France
[e] Engine Research Laboratory, Caterpillar Inc., Mossville, IL 61552, USA
[f] Hino Motors, Ltd., Tokyo, Japan

## HIGHLIGHTS

- Characterization results of the Engine Combustion Network's Spray C & Spray D injectors.
- Analysis of the spray, combustion, and soot formation for the Spray C & Spray D injectors.
- Comparison between the results obtained by three different research institutes.
- A novel method for quantitative soot results based on volume is presented.
- An injector with promoted cavitation produces more or less soot depending on ambient temperature.

## ARTICLE INFO

*Keywords:*
Engine Combustion Network (ECN)
Spray C & Spray D
Cavitation
Lift-off length
Ignition delay
Soot extinction imaging

## ABSTRACT

In a collaborative effort to identify key aspects of heavy-duty diesel injector behavior, the Engine Combustion Network (ECN) Spray C and Spray D injectors were characterized in three independent research laboratories using constant volume pre-burn vessels and a heated constant-pressure vessel. This work reports on experiments with nominally identical injectors used in different optically accessible combustion chambers, where one of the injectors was designed intentionally to promote cavitation. Optical diagnostic techniques specifically targeted liquid- and vapor-phase penetration, combustion indicators, and sooting behavior over a large range of ambient temperatures—from 850 K to 1100 K. Because the large-orifice injectors employed in this work result in flame lengths that extend well beyond the optical diagnostics' field-of-view, a novel method using a characteristic volume is proposed for quantitative comparison of soot under such conditions. Further, the viability of extrapolating these measurements downstream is considered. The results reported in this publication explain trends and unique characteristics of the two different injectors over a range of conditions and serve as calibration targets for numerical efforts within the ECN consortium and beyond. Building on agreement for experimental results from different institutions under inert conditions, apparent differences found in combustion indicators and sooting behavior are addressed and explained. Ignition delay and soot onset are correlated and the results demonstrate the sensitivity of soot formation to the major species of the ambient gas (i.e., carbon dioxide, water, and nitrogen in the pre-burn ambient versus nitrogen only in the constant pressure vessel) when holding ambient oxygen volume percent constant.

## 1. Introduction

Emissions of particulate matter (PM) and nitric oxides ($NO_x$) from compression-ignition engines have been curbed significantly over the past few decades. In recent years, this reduction in pollutant emissions has been accompanied by a simultaneous increase in brake thermal efficiency. Yet, driven by legislation and demand for cleaner internal combustion engines with a concurrent reduction in fuel consumption,

* Corresponding authors at: Combustion Research Facility, Sandia National Laboratories, P.O. Box 969, MS 9053, Livermore, CA 94551, USA
*E-mail addresses:* n.c.j.maes@tue.nl (N. Maes), lmpicke@sandia.gov (L.M. Pickett).

https://doi.org/10.1016/j.applthermaleng.2020.115136
Received 6 December 2019; Received in revised form 27 January 2020; Accepted 27 February 2020
Available online 02 March 2020

there is a need for an improved understanding of the in-cylinder processes that dictate engine-out emissions. Although contemporary diesel particulate filters (DPFs) can effectively reduce soot emissions up to 90% below legislation limits, the filters eventually become clogged and require regeneration [1]. Regeneration involves additional fuel injection events to elevate the exhaust gas temperature and initiate oxidation reactions, while the emissions may increase significantly during the process [2]. This additional fuel consumption ultimately leads to fuel efficiency penalties. While the DPF may be a permanent component on all future diesel engines, its size, cost, and the frequency of regeneration may be reduced by improving the in-cylinder combustion characteristics through a better understanding of the processes leading up to pollutant formation.

Improved fuel/air mixing prior to the time of high-temperature ignition or upstream of the location where a mixing-controlled diesel jet flame stabilizes (i.e., the lift-off length) has been shown to be effective in reducing soot emissions [3,4]. In this work, the cavitation phenomenon that diesel injectors experience when the pressurized fuel is forced around sharp edges is studied to understand its effect on spray- and soot formation, while noting that severe cavitation is known to damage injectors [5–9].

Due to the strong change in direction of a cavitating flow, boundary layer separation and a recirculation zone arise, in which a depression with local pressures below the vapor pressure of the fuel exist [6]. The vapor-phase recirculation zone causes a flow acceleration because of the imposed area restriction for the main flow. Cavitating fuel sprays tend to have a higher near-field spreading angle, signifying enhanced mixing [10,11]. As fuel pressures of present-day injection equipment rise to enhance mixing and air entrainment, the likelihood of encountering cavitating regimes also increases.

To leverage the improved mixing to the advantage of soot reduction following the guidelines described by Pickett et al. [3], the cavitation enhanced mixing must not be negated by a decrease in flame lift-off length. In this aspect, the higher exit velocity from the flow acceleration may help to restore or increase the lift-off length again because of their direct correlation [12]. Alternatively, a parameter such as ambient temperature does not influence mixing [13], while it does have a huge impact on the combustion processes. This means that a concerted optimization of various parameters could be required to utilize the improved mixing that comes with cavitation. In a study by Payri et al. [14], cavitation effects on the lift-off length and soot formation processes are analyzed using a conical and a cylindrical hole. In their study, Payri et al. show how the cavitating cylindrical hole reduces the effective diameter and increases the LOL. Therefore, the equivalence ratio at the lift-off length is reduced, resulting in less soot. In the numerical study by Som et al. [9], a hydroground injector is reported to produce less soot compared to an identical straight-hole version with severe cavitation, which they ascribed to a smaller rich-premixed combustion zone. On the contrary, another injector with a conical (or converging tapered) hole that also decreases the amount of cavitation, and the mass flow due to the reduced exit orifice diameter, produces more soot than the identical straight-hole version while injecting less fuel. Their findings are based on a relatively reactive environment with a fixed ambient temperature of 1000 K and an ambient oxygen concentration of 21% $O_2$, and it appears that there are confounding effects. Due to the aforementioned requirement of a concerted optimization, these results may very well change when the reactivity of the ambient changes. Therefore, high-fidelity simulations which are validated using reproducible experiments can play an important role for future engine design.

To facilitate the understanding of events and features that impact the operation of heavy-duty compression ignition engines, the Engine Combustion Network (ECN) has established reference conditions with two single-hole, heavy-duty diesel injectors. One of the injectors was designed to promote cavitation with sharper edges and a straight hole, while the other injector has a converging hole and was subjected to hydro-erosive grinding to eliminate sharp edges. For these specific injectors, fluctuations in the recirculation zone and phase change at the exit of the cavitating orifice have previously been identified by an increase in the spreading angle and a corresponding reduction in flame lift-off length [10,11].

In addition to the potential enhancement in mixing, a certain degree of cavitation may prevent deposit formation inside injection equipment [15]. Such deposits, referred to as coking, affect spray behavior over time and subsequently engine performance and emissions. While some amount of cavitation may therefore be desirable to avoid injector deposits, excessive cavitation can lead to injector erosion and the aforementioned damage to equipment. Such tradeoffs illustrate the delicate balance and risk involved with the subject matter [16].

Comparing experimental results obtained by individual research institutes with nominally identical injection equipment lends greater confidence in the accuracy of the obtained results and identifies uncertainties originating from small perturbations in boundary conditions [17–19]. Such confidence and accuracy is valuable for numerical simulations, which is borne out by various recent computational studies within the ECN (e.g. [20–27]). In this study, the sprays were studied in a constant-pressure, high-throughput facility at the Spray Combustion Laboratory at Caterpillar, as well as in constant-volume pre-combustion vessels at Sandia National Laboratories (SNL) and IFP Energies Nouvelles (IFPEN). In previous collaborative efforts, the ambient conditions in these facilities as well as combustion indicators and flame structures of reference cases with a small orifice injector (90 μm, classified as “Spray A”) were studied [17–19].

Techniques to visualize spray penetration and primary combustion indicators for fuel sprays are well established and standardized methods have been recommended in recent years [19,28,29]. Concerning particulate matter formation and consumption, diffused back-illumination (DBI) extinction imaging has emerged as a cost-effective, and relatively simple approach for high-speed soot analysis and quantification [30]. As the so-called “Spray C” (C for cavitation), and “Spray D” injectors used in this work have relatively large orifices, between 190 and 212 μm, compared to the previously characterized Spray A reference, they inherently produce larger sprays with more soot. Due to the resulting increase in optical thickness, relatively large incident wavelengths of 623 nm and 850 nm are used in this work compared to previous work (e.g. between 400 nm and 520 nm in references [31–34]). Using longer incident wavelengths reduces molecular absorption, and decreases the dimensionless extinction coefficient $k_e$ according to the Rayleigh-Debye-Gans (RDG) theory [31,35,36]. In this work, recommendations for the $k_e$ values provided by Skeen et al. are used to relate the measured optical thickness values to soot mass [36].

The ECN provides standardized target conditions for diesel spray experiments including fuel type, temperature, and injection pressure as well as ambient density, ambient temperature, and ambient oxygen concentration. For ECN experiments conducted in a pre-burn type vessel, the pre-burn gas composition determines the ambient composition of gases prior to liquid fuel injection. In constant-pressure vessels associated with the ECN, the ambient composition at the time of liquid fuel injection is specified as either air or nitrogen-diluted air—although dilution with $CO_2$ and water to simulate exhaust gas recirculation (EGR) is feasible but has not yet been implemented. At Sandia and IFPEN, the pre-burn gas compositions were comparable leading to consistent ambient mixtures containing 15% $O_2$, and about 3.8% $H_2O$, and 6.5% $CO_2$ by volume. For the experiments conducted at Caterpillar, only $O_2$ and $N_2$ were present in the ambient. For mixing and ignition/flame stabilization processes in these high-pressure spray flames, small changes in ambient composition appear to be inconsequential for ignition and lift-off length [17]. However, there is evidence that such changes may have an important effect for soot formation. In several diffusion-flame studies, soot formation is reduced by the addition of $CO_2$ and $H_2O$ to the ambient [37–40]. In addition to a reduced adiabatic flame temperature, the reverse reaction of $OH + H_2 \rightleftharpoons H + H_2O$

produces OH radicals that can help oxidize soot [41]. On the contrary, soot emissions from internal combustion engines may eventually increase with the presence of water when using EGR [42–44]. To address the specific effect of $CO_2$ and $H_2O$ on soot formation, experiments in a rapid compression machine were performed using different levels of $CO_2$ and $H_2O$ [45]. For a 0.09-mm Spray A injector, it was observed how an ambient composition representative for a pre-burn combustion vessel preconditioning reduced the amount of soot produced by a 0.09-mm Spray A injector by 50% when compared to an environment with only $N_2$ and $O_2$.

When comparing the present data to experiments in actual internal combustion engines, one needs to consider the fact that in engines, other processes play a role as well. When the water and carbon dioxide content of the inlet gas is increased, the end-compression temperature will be reduced due to the higher heat capacity. In addition, increased EGR percentages reduce oxidizer availability, thereby limiting soot oxidation. Indeed, using numerical simulations to substantiate increased soot emissions from experimental data, Ni and Wang show how soot formation is reduced early in the cycle, but oxidation deteriorates due to reduced oxygen content and lower combustion temperatures [42]. Using laser extinction and in-cylinder gas sampling, Gallo et al. confirmed how soot oxidation reduced with decreasing oxygen percentages [44], which they ascribed to a reduction in OH radical production at a lowered adiabatic flame temperature. In the case of a constant-volume or constant-pressure facility, temperature and oxygen percentage are decoupled, thus isolating the effects of ambient composition. The composition itself, however, cannot easily be changed, as may be the case in a counter-flow or co-flow diffusion flame. Somewhere in-between, Musculus et al. show how using a water-diesel fuel emulsion shows potential for the simultaneous reduction of soot and $NO_x$ in the exhaust [46]. The reduction of $NO_x$ emissions is governed by a reduced flame temperature at all operating conditions. The increased premixing of fuel and air during the premixed burn and mixing-controlled combustion phase may reduce particulate matter formation, but liquid fuel impinging on the wall may result in an increase of CO, HC and PM emissions.

In this work, effects of cavitation on spray penetration, combustion characteristics and soot formation of n-dodecane sprays are considered. While spray and combustion parameters obtained in the Sandia combustion vessel for Spray C and Spray D were previously compared by Westlye et al. [10], the present study uses new data with updated measurement and processing techniques. In addition, soot results are included, and all results are compared to those obtained at IFPEN and Caterpillar. Spray penetration results are first used to validate consistency in physical spray behavior. In addition, these results are used to predict fuel mixture fraction fields that, together with the obtained combustion indicators, substantiate findings with respect to soot values [47]. As shown in previous studies [48,49], soot formation decreases with increased lift-off length and the associated decrease in equivalence ratio at the lift-off length until an equivalence ratio of approximately 2. For equivalence ratios below 2, soot is no longer formed in the fuel jets of these references. In this study the ambient temperature representative for compression ignition engines is varied between 850 K and 1100 K. Ambient temperature was intentionally chosen as an isolated variable without altering fuel vapor dispersion [13]. The study provides new understanding as to how cavitation influences fuel-air mixing, ignition, high-temperature heat release, and soot formation for different gas temperature and pressures.

## 2. Experimental facilities and injection equipment

Three individual experimental setups have been employed to compare the different injectors in this work at the high-temperature and high-pressure conditions representative for compression ignition engines. The used setups can be subdivided into two categories, which use either a pre-burn of a combustible mixture or a continuous heated flow to achieve the desired ambient environment. The experimental setups used in this work were compared and characterized extensively, as detailed by Meijer et al. [18].

For the pre-burn combustion approach, target conditions are reached by igniting a combustible mixture in the closed volume via a spark discharge. For IFPEN, the gas mixture is filled sequentially and contains 6.7% $CO_2$ and 3.9% $H_2O$ by volume after the pre-burn event when 15% $O_2$ is targeted. Compared to arriving at an oxygen percentage of 15% using approximately 38% of ideal EGR, this means that there is even an additional amount of $CO_2$ present in the ambient gas [18]. Sandia gas mixtures were prepared external to the laboratory prior to experiments. The gas mixtures are subsequently used for multiple filling sequences, and the ambient gas prior to injection contains 6.2% $CO_2$ and 3.6% $H_2O$ by volume. In the high-throughput vessel of Caterpillar, the heated flow is composed purely out of $N_2$ and $O_2$ when the fuel injection starts.

Single-orifice, solenoid-activated injectors belonging to the Spray C and Spray D family of the ECN were used in this work to study sprays of n-dodecane. Fuel injection equipment details for the different institutes are listed in Table 1. The orifice diameters reported here correspond to the values measured at the nozzle outlet, although the minimum diameters are located inside the holes [10]. The detailed three-dimensional

**Table 1**
Fuel injection equipment details and soot extinction system features for experiments performed at IFPEN, Sandia and Caterpillar. Double values, when presented, represent independent entries for Spray C and Spray D.

| | Sandia | Caterpillar | IFPEN |
|---|---|---|---|
| Injectors | C037 & D134 | C037 & D134 | C003 & D135 |
| Injector driver | Genotec | National Inst. driven | EFS IPoD |
| Mass flow [g/s][a] | 10.10 & 11.95 | 10.10 & 11.95 | 10.26 & 11.49 |
| Orifice exit diameter [$\mu$m][a] | 208 & 191 | 208 & 191 | 212 & 190 |
| Effective diameter [$\mu$m][b] | 179 & 191 | 179 & 191 | 180 & 188 |
| Hydraulic delay [$\mu$s][c] | 361 & 380 | 400 | 440 |
| Light source [nm] | 850 - LED | 623 - LED | 810 - Laser |
| Extinction coefficient $k_e$ [–] | 5.0 | 7.2 | 5.5 |
| Extinction cross section $C^*$ [$\mu m^2$] | 7.04 | 4.08 | 7.27 |
| Filtering [nm] | OD2.3, 850 ± 5 | OD2, 628 ± 16 | OD2, 810 ± 2 |
| Camera | Phantom V2512 | Phantom V2512 | Photron SA-Z |
| Maximum FOV [mm] | 70 | 73 | 67 |

[a] Values from Payri et al. [50], corresponding to an injection pressure of 150 MPa.
[b] The effective diameters here are computed by multiplying the orifice exit diameter by the square root of the area coefficient at an injection pressure of 150 MPa. Again, the values from Payri et al. were used [50].
[c] Values do not vary between injectors for identical injector driver and driver settings according to Payri et al. [50].

internal nozzle geometries for these injectors can be found online [51]. Note that all injectors in this table were characterized to have an identical hydraulic delay in a previous study (440 μs) [50] when controlling the injector body to 343 K. From the results shown in this table, however, it does appear that these values depend on the installation or the injector driver used, with a maximum difference of nearly 80 μs between different institutes. To account for these hydraulic delay differences, all spray data will be analyzed relative to the time when liquid injection commences. While parametric variations in ambient temperature and injection pressure were conducted for this publication, the base-line ambient condition is a 150-MPa injection into a 900-K ambient with a density of 22.8 kg/m$^3$.

## 3. Diagnostic techniques and measurements

Despite differences in experimental combustion vessels, very similar or even identical optical diagnostic technique setups were used in this work. The following sections detail the setups that were used to visualize spray penetration, combustion indicators, and soot formation in the different combustion facilities. Several high-speed movies from the Spray C and Spray D dataset have been made available on the ECN website [52].

### 3.1. Schlieren imaging

IFPEN and Sandia recorded images of the vapor-phase n-dodecane fuel to characterize non-reacting spray penetration for both injectors. IFPEN used a continuous-wave white LED with two condensing lenses (an f = 200 mm spherical lens and a Fresnel lens) to direct the emission through a primary 0.5-mm pinhole, which was selected after a trial and error optimization. Two f = 500 mm spherical lenses are mounted close to the vessel to obtain a collimated light-beam in the test section. A second 0.5-mm aperture mounted in the focal-points of the schlieren lens after the test section is used to block large-angle light refraction, similar to Ref. [32]. Spray images were collected using a high-speed CMOS camera (Photron SA-Z) at 36 kfps with a 5.1-μs exposure time. An 85-mm f/1.4 lens equipped with a 600-nm short-wave-pass filter provided a projected pixel size of 0.13 mm/pixel.

Sandia used a Z-type schlieren setup as described in Ref. [53]. Pulsed light from a 630-nm custom LED (15-nm FWHM) was collected and focused by a condensing lens through a 3-mm aperture. The extended source was then collimated by a 115-mm diameter, f/8 parabolic mirror and directed through the vessel and onto a second identical parabolic mirror with a series of flat folding mirrors. The second parabolic mirror focused the collimated light for collection by a high-speed CMOS camera (Photron SA-X2). The camera was operated at 150 kfps with a 5.6-μs exposure and was equipped with an 85-mm f/1.4 lens and a 628-nm (32-nm FWHM) band-pass filter. By using a spectrally narrow light-source and band-pass filter, incandescent light was rejected for additional recordings with an oxygen percentage of 15% to study reacting spray penetration.

### 3.2. OH* chemiluminescence imaging

High-speed OH* chemiluminescence was used to visualize high-temperature reactions, and to determine combustion indicators such as the flame lift-off length and ignition delay in all experimental facilities. Note, however, that especially due to the sooting propensity of the large-orifice injectors, significant amounts of incandescent soot will be present in such images, limiting interpretation to the flame lift-off region [54]. At IFPEN, a high-speed CMOS camera (Photron SA-Z) was lens-coupled to a high-speed image intensifier (Lambert HiCATT, S20 photocathode) and the system was operated at 75 kfps with a 12.3-μs exposure. Although resolution is certainly limited by the image intensifier in this case, a projection of 0.11 mm/pixel was imaged on the camera. Light was collected through a Semrock band-pass filter set centered around 315 nm (20-nm FWHM) and a 100-mm f/2.8 Sodern Cerco UV lens. Sandia used the same high-speed equipment, but with a 105-mm f/4.5 UV Nikkor lens and a 312-nm (16-nm FWHM) band-pass filter combined with a 358-nm short-wave-pass filter. Undesired broadband emission in the Sandia movies was reduced further by redirecting flame emission off of a 308 nm high-reflector mirror. The Sandia system was operated at 50 kfps with an intensifier gate time of 10 μs and was characterized by a projected pixel size of 0.105 mm/pixel. At Caterpillar, a Video Scope (VS4-1845HS) intensifier was lens-coupled to a phantom V710 and light was collected through a 105-mm f/4.5 UV Nikkor lens at f/16 and a 308-nm (10-nm FWHM) band-pass filter and a UG11. Similar to Sandia, a 308-nm mirror was used as a first separator for the OH* chemiluminescence signal. The Caterpillar system was operated at 19 kfps with an exposure time of 50 μs and a projected pixel size of 0.268 mm/pixel.

### 3.3. Pressure analysis

For the constant-volume combustion facilities, in-vessel pressure is measured using a pressure transducer mounted in one of the diagonal corner ports. Governed by heat-loss to the walls, in-vessel pressure gradually decays after the pre-combustion event. In order to isolate the pressure-rise originating from the injected fuel spray, exponential fits over a range of 100 ms before and after the injection event are used to correct for the cool-down trends. As these trends are different before and after the event of interest when large quantities of fuel are injected, a seamless transition between pre-injection and post-combustion fit is used based on an initial net-pressure increase using just the pre-injection fit. A speed of sound correction is applied based on the lift-off location for each operating condition, to correct for the distance between the ignition site and the pressure transducer [54–56]. Pressure traces are filtered using a low-order smoothing procedure, and ensemble-averaged afterwards. Results from both combustion vessels are post-processed using an identical routine, with exception of filtering options due to the different acquisition rates used by Sandia (100 kHz) and IFPEN (200 kHz).

### 3.4. Diffused back-illumination extinction imaging

The DBI extinction setups used in this study all feature a pulsed light source. The emission of these light sources is intentionally diffused to obtain a quasi-Lambertian distribution, and directed through the spray vessels towards a high-speed camera [30]. A schematic overview of the DBI extinction setup as applied by Sandia is shown in Fig. 1. This method minimizes beam steering effects due to refractive index gradients near the vessel windows and by the spray, while liquid phase fuel and soot provide sources for light extinction.

The camera may be synchronized with the pulsed light source for liquid fuel imaging, but it is operated at twice the frequency for soot imaging. This way, a background image is recorded between each extinction frame, which is used to correct for local incandescent soot

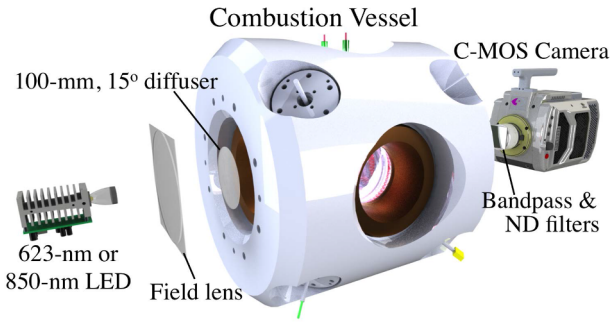


**Fig. 1.** Schematic overview of the diffused back-illumination extinction imaging setup as implemented at Sandia.

radiation. The (corrected) extinction images are used to compute the optical thickness ($\tau$) according to Beer-Lambert,

$$\tau = -ln(I/I_0). \tag{1}$$

In this equation, $I$ is the transmitted intensity and $I_0$ is the intensity when there is no extinction. Regions in which extinction does not take place during the entire duration of the experiment are typically used to correct for changes in recorded pixel-to-pixel background intensity. Note that both the illumination intensity as well as the camera sensitivity might change over the course of a recording. The liquid DBI extinction data can be quantified as projected liquid volume fraction (*pLVF*) using

$$pLVF = \int_{-\infty}^{\infty} LVF \cdot dy. \tag{2}$$

Based on Mie-theory the optical thickness $\tau$ can be related to the liquid volume fraction (*LVF*) as

$$\tau = \int_{-\infty}^{\infty} C_{ext}^{*} \frac{LVF}{\pi d^3/6} dy, \tag{3}$$

where $C_{ext}^{*}$ is the droplets extinction cross section that depends on the droplet diameter, the refractive index $n_{fuel}$ of the media, the incident wavelength $\lambda$, and the collection angle of the optical setup. By assuming a mono-dispersed spray $C_{ext}^{*}$ is constant along the line of sight and Eq. (3) can be rewritten as,

$$\tau \frac{\pi d^3/6}{C_{ext}^{*}} = \int_{-\infty}^{\infty} LVF \cdot dy = pLVF. \tag{4}$$

The value of $C_{ext}^{*}$ can be obtained for individual experimental setups using MiePlot [57]. In this case, the assumption is made that nominally identical injectors with standardized fuel and ambient boundary conditions will result in the same droplet diameter near the liquid length. The threshold chosen to determine the liquid length based on this procedure is $pLVF = 0.2 \cdot 10^{-3}$ mm$^3$ liquid/mm$^2$, consistent with recommendations in the ECN guidelines [51]. In this way the extinction results obtained in experiments performed by different research institutes are related to a physical parameter that depends entirely on the spray, and that can be compared among experiments and numerical simulations.

The quantification of soot from extinction imaging experiments is desired for meaningful comparison between different setups and to numerical efforts too. From an experimental perspective, this is because of the dependence of the optical thickness on wavelength. Translating optical thickness values to soot volume fraction or soot mass requires knowledge about both the optical and physical properties of the soot particles. A convenient method is to determine the soot mass per pixel according to

$$m_{soot,pixel} = \lambda \cdot \tau \cdot \rho_{soot} \cdot A_{pixel} / k_e, \tag{5}$$

in which $\lambda$ is the incident wavelength, $\rho_{soot}$ is the density of soot particles, and $k_e$ is the dimensionless extinction coefficient. The dimensionless extinction coefficient depends on both optical, as well as morphological properties of soot. Recently, Skeen et al. recommended a range of non-dimensional extinction coefficient ($k_e$) values for soot measurements in high-pressure combusting sprays [36]. Their recommendations are based on a comparison of soot measurements in a high-pressure spray with DBI extinction experiments performed in a well-characterized, steady, laminar diffusion flame. They asserted that soot particles in the two flame configurations having similar primary particle sizes, similar morphological properties, and characterized by similar $k_e$ ratios at two distinct wavelengths should have consistent optical properties. After determining $k_e$ in the laminar diffusion flame at a location where the above requirements were met for a range of incident wavelengths extending from the near-ultraviolet to the near-infrared, they recommended a set of wavelength dependent $k_e$ values for use in high-pressure sprays. Naturally, these values can be used to interpolate and find $k_e$ values at different wavelengths as well, which will be used to evaluate the soot mass in a coherent way in this work. The used values, and some additional details of the optical setups are listed in Table 1. At Sandia, a custom infrared high-speed LED centered at 850 nm was operated at 50 kHz and directed towards a high-speed camera (Phantom V2512) operating at 100 kHz as illustrated in Fig. 1. Experiments at Caterpillar were conducted using a red LED (centered at 623 nm) at 50 kHz. The camera (Phantom V2512) was operated at 100 kHz with a 1.6-μs exposure and was equipped with an 50-mm f/1.2 lens, a 628-nm (32-nm FWHM) band-pass filter, KG3 Schott glass filter, and a 500D close-up lens. For the DBI system at IFPEN, a 810-nm diode laser (Cavitar Cavilux HF) was operated at 25 kHz with a pulse-width of 0.26 μs, while a high-speed camera (Photron SA-Z) was operated with double the frame speed and an exposure time of 0.35 μs. In all cases, a combination of neutral density filters and band-pass filters was used to reject as much flame luminosity as possible, while transmitting the incident light.

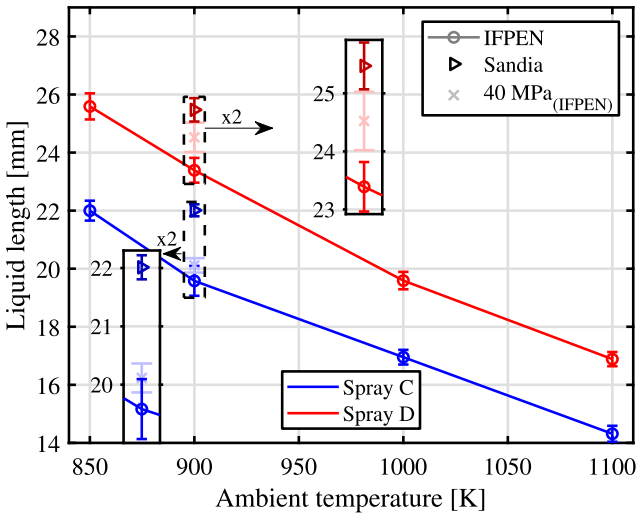


**Fig. 2.** Liquid length values obtained from inert experiments between 1 and 3 ms aSOI for different ambient temperatures, and additional cases with an injection pressure of 40 MPa. Error bars indicate 95% confidence intervals using a t-distribution.

## 4. Results and discussion

### 4.1. Liquid fuel penetration

Using the procedure for projected liquid volume fraction described above, liquid length values were evaluated based on a time-averaged result between 1 and 3 ms after SOI for different ambient temperatures at IFPEN (Fig. 2). The error bars in this figure show 95% confidence intervals based on a t-distribution. Values obtained with an injection pressure of 40 MPa (large error bar cap), and baseline Spray C and Spray D values by Sandia are indicated as well. The difference between Sandia and IFPEN data is rather significant, and is similar to a 50-K ambient temperature difference in the results by IFPEN. Fuel temperature, however, has a more pronounced influence on the liquid length [58,59], while determining this temperature at the orifice involves more uncertainty [60]. Based on the data by Payri and coworkers, and Siebers, the shown decrease in liquid length would correspond to a fuel temperature difference of about 40 K [58,59].

Although the dependence of liquid length on the ambient temperature has been described in previous work by Siebers [61], Fig. 2 illustrates how the values found for Spray C are consistently approximately 4 mm shorter across the different conditions, as was shown by Westlye et al. [10]. Based on the work by Siebers, one can expect a near-linear relationship between the orifice diameter and the liquid

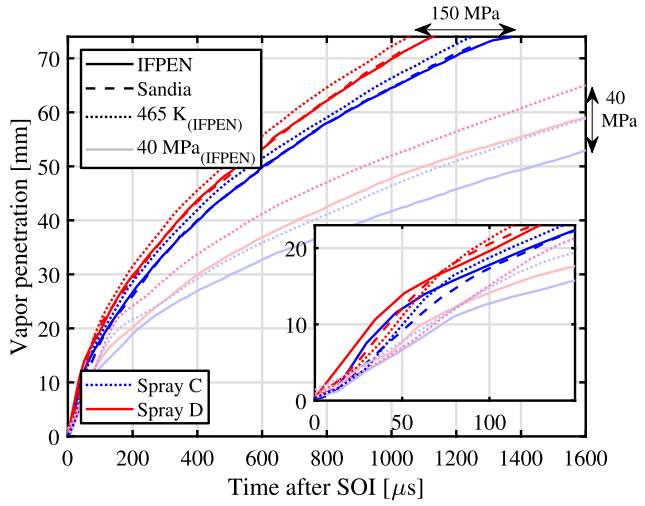


**Fig. 3.** Comparison of spray penetration results obtained at IFPEN and Sandia. Ambient temperature and density are 900 K and 22.8 kg/m$^3$, respectively, while the injection pressure is 150 MPa. For IFPEN, results of an injection pressure of 40 MPa, and an ambient temperature of 465 K are shown as well.

length. However, the small reduction of effective orifice diameter (see Table 1, amounting to 4% for the IFPEN injectors) does not account for the 4 mm decrease in liquid length, which indicates that cavitation plays an important role here [10]. Furthermore, the figure illustrates how even the pressure difference of 110 MPa results in a relatively small influence on liquid penetration, due to the balance between mixing and momentum [61,62].

### 4.2. Spray penetration

Fuel vapor penetration measurements are used to confirm similar spray and mixing behavior between ambient conditions with the nominally identical injectors. Additionally, the vapor penetration and nozzle momentum and mass flow are used as inputs to predict local equivalence ratio via the 1D spray model described by Musculus and Kattke [47]. Fig. 3 shows how the vapor penetration curves of Sandia and IFPEN practically overlap for an injection pressure of 150 MPa. As demonstrated in past work [10], tuning the spray spreading angle to match penetration and accounting for differences in nozzle flow coefficients provides a means for mixing comparison between Spray C and Spray D. The strong agreement in vapor penetration between institutions provides confidence in the mixing field assessment, but additional analysis of changes in cavitation and the impact on nozzle flow coefficients or penetration with different operating conditions can be assessed.

An expression for the role of cavitation on nozzle flow is $K$, as defined by Nurick [63]. This number is used in an exercise to evaluate whether cavitation is diminished for the spray C injector when the pressure drop over the injector is decreased, or whether Spray D is expected to show cavitation effects at a greater pressure drop. The number depends on the injection pressure ($p_i$), the ambient- or backpressure ($p_b$) and the vapor pressure of the fuel ($p_v$) according to

$$K = \frac{p_i - p_v}{p_i - p_b}. \tag{6}$$

Table 2 shows the cavitation number for the Spray C and Spray D baseline, and extreme variations with reduced injection pressure and ambient temperature as tested in the IFPEN combustion vessel. In addition, reference cases that have similar values with available nozzle flow coefficients are shown. When $K$ falls below a certain, injector-specific value, mass flow asymptotes and no longer depends on the pressure drop over the injector [6,63]. For an injection pressure of 40 MPa, a diminished effect of cavitation is expected due to the reduced pressure drop. However, the difference between Spray C and Spray D remains similar, indicating that cavitation effects are not yet obviated for Spray C, even at the lowest attainable injection pressures. This is confirmed when evaluating the available data at an injection pressure of 50 MPa, since the effective orifice diameter is still smaller than the exit orifice diameter and minimum diameter for injector C003. With only a minor decrease of 10 MPa, no difference is expected yet. When the 150 MPa injections take place in a cold environment (465 K, IFPEN only), $K$ decreases due to the reduced ambient pressure at a fixed density (3.12 MPa and 22.8 kg/m$^3$, respectively). The difference between the two injectors is now apparent for these cases, showing that the Spray D injector is not sufficiently close to the collapsed mass flow regime to cause a noticeable deviation. From the available data with a backpressure of 2 MPa (lowest $K$), the effective diameter is very close to

**Table 2**
Nurick's cavitation number $K$ for baseline Spray C and Spray D experiments at 900 K with a density of 22.8 kg/m$^3$, a low injection pressure case, and a case with a lower ambient pressure ("cold"). As a reference the lowest injection pressure case for which flow coefficients are available (50 MPa), and a case with even lower backpressure (2 MPa) are reported. Effective diameters for the injectors used by IFPEN are shown similar to Table 1 for the cases with available flow coefficients.

| | Baseline | Low $p_i$ | Cold | Ref. 50 MPa | Ref. Low $p_b$ |
|---|---|---|---|---|---|
| $p_i$ [MPa] | 150 | 40 | 150 | 50 | 150 |
| $p_b$ [MPa] | 6.04 | 6.04 | 3.12 | 6.04 | 2.00 |
| K [–] | 1.042 | 1.178 | 1.021 | 1.137 | 1.01 |
| $d_{eff}C$ | 180.2 | | | 185.0 | 177.2 |
| $d_{eff}D$ | 188.2 | | | 186.1 | 185.6 |

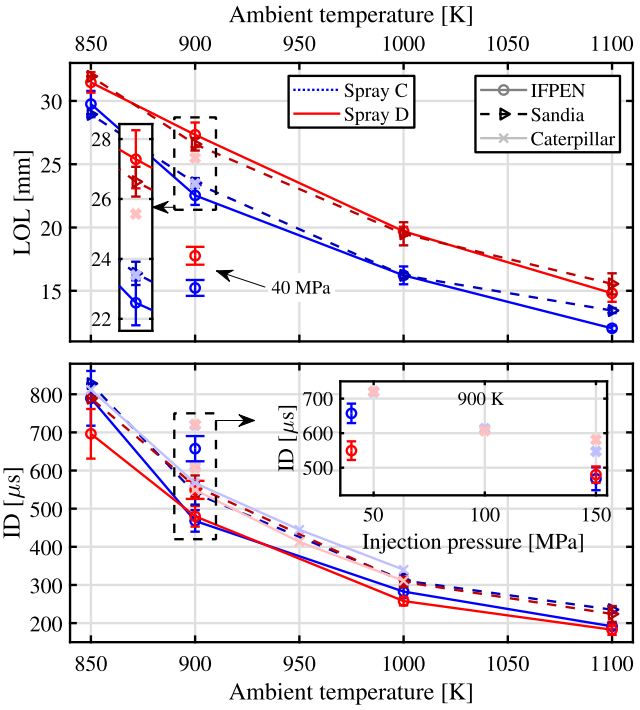


**Fig. 4.** Flame lift-off length and ignition delay for different ambient temperatures. Error bars indicate 95% confidence intervals using a t-distribution. At an ambient temperature of 900 K, results from all three institutes, with additional injection pressure variations are shown in the inset. For the ignition delay values at 900 K, an additional inset is included that shows the dependence on injection pressure. Note that Caterpillar ignition delay values were obtained from head-on high-speed images of the spray combustion event collected through a 550-nm short pass filter.

the effective diameter of the case with 50 MPa injection pressure ($K$ = 1.37). Therefore, it is not expected that even the lowest ambient temperature of 850 K (for which $K$ = 1.038) will yield different mixing behavior, leading to differences in combustion and soot formation that are not related to the ambient temperature effect.

### 4.3. Ignition delay and lift-off length

A comparison of ignition delay (ID) and lift-off length (LOL) values as a function of temperature is reported in Fig. 4. For Caterpillar, ignition delay data is derived from head-on visible chemiluminescence, rather than high-speed OH*. Error bars in this figure represent 95% confidence intervals using a t-distribution. To improve the comparison, lift-off length values were derived using an identical approach, according to ECN guidelines [51]. For this approach, a 50% threshold of the maximum intensity in the lift-off region is used independently above and below the spray axis to find a lift-off length. The average between these two axial distances is subsequently used as a final value. For these specific injectors, Spray C shows a lift-off length that is on average 3 mm shorter than the Spray D values over a wide range of conditions. Again, this is more than a 1.5% difference as predicted by power-law relationships for the lift-off length in combination with the effective diameters from Table 1 [12]. This result is consistent for all institutions, and indicates the influence of cavitation on lift-off length. For higher ambient temperatures, the liquid length is longer than the lift-off length, although the liquid is confined to the center of the plume while lift-off stabilizes toward the stoichiometric location on the jet periphery. At lower ambient temperatures, below 950 K, the lift-off length is longer than the liquid length. Also, the liquid length does not change with injection pressure, while the lift-off length is significantly reduced for the 40-MPa injection case [61].

Combustion also does not significantly alter liquid penetration either. Comparing liquid length values of IFPEN between reacting and non-reacting fuel sprays, the liquid length reduces by a small amount, less than 5%, for all temperature variations (also shown by Westlye et al. [10]), including those with a lift-off length shorter than the liquid length. As mixing with hot combustion products would be expected to increase evaporation and shorten the liquid length, the finding that there is little effect suggests that little hot combustion products reach the liquid region and liquid-flame interactions are minimal or non-existent. Part of this observation could be the result of the decreased air entrainment associated with heat release in a jet [64–66]. However, the equivalence ratio at the location of the lift-off will become increasingly fuel-rich for the cases where the lift-off length is shorter than the liquid length, which will intensify soot formation [48].

Another consideration to explain the lift-off length trend for Spray C versus Spray D is the effect of the jet spreading angle, as described in [10]. Spray C has a larger spreading angle, which partially explains the slower penetration shown in Fig. 3. A larger spreading angle produces slower moving mixtures at the jet periphery near stoichiometric positions. From the standpoint of either ignition-timing stabilization or flame speed [23], a fuel jet with a larger spreading angle (i.e., Spray C) will stabilize closer to the injector. Indeed, examination of the ignition delay data shows roughly the same ignition delay for Spray C and Spray D for a given operating condition and institution. The igniting region of Spray C, with a larger spreading angle, is therefore likely to be closer to the injector for subsequent lift-off stabilization.

#### 4.3.1. Pressures based ignition

Despite the similarities obtained for the lift-off length values, measured ignition delays by chemiluminescence are 10–20% lower for IFPEN compared to Sandia (Fig. 4). Additional ignition delay data derived from measured pressure will be discussed below in order to further explore these differences. Fig. 5 shows the net pressure increase after the start of injection for Spray C and Spray D experiments in the constant-volume vessels. The IFPEN data is scaled with a factor 1.19 to correct for the pressure-rise rate difference induced by the different vessel volumes. A longer injection duration for IFPEN experiments results in more injected mass and therefore a higher net pressure increase.

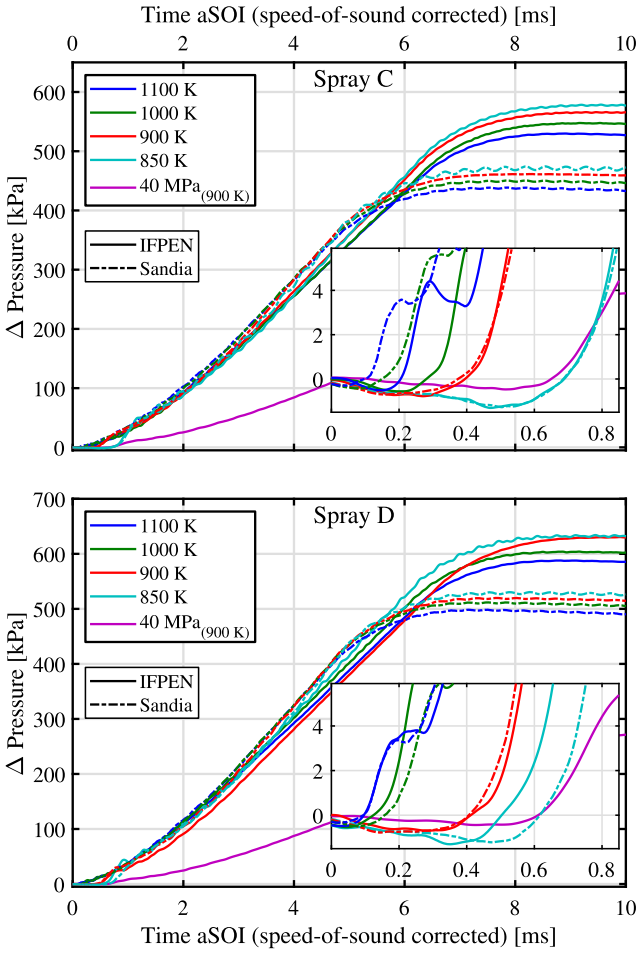


**Fig. 5.** Ensemble-averaged net pressure increase in constant-volume combustion vessels at different ambient temperatures. The curves with a 40-MPa injection pressure correspond to an ambient temperature of 900 K. The data obtained at IFPEN has been scaled to correct for the pressure rise rate difference caused by different vessel volumes.

Evaluating the effect of increasing ambient temperature on the net pressure increase after the end of combustion, shows a reduced pressure-rise. Especially at these higher ambient temperatures, variations in combustion efficiency are expected to be negligible, and the pressure traces are corrected for the global heat-release of the combustion vessels. Conversely, the flame length reduces with increasing ambient temperature—therefore reducing flame quenching at the vessel boundary. However, the flame temperatures will be significantly higher for the increased ambient temperature, and it is expected that this causes a significantly higher local heat-flux through the vessel window opposite from the injector [67,68].

The determination of ignition delay based on net pressure increase requires the definition of a threshold, which was found to be around the order of 3 kPa for Spray A experiments to match the values obtained by high-speed chemiluminescence measurements. Because of the greater volume in which ignition may take place, and the larger quantities of fuel that contribute to first- and second-stage heat release, suitable definitions for the ignition delay have yet to be established. The inset in each panel of Fig. 5 highlights the time shortly after the start of injection, indicative for the ignition process. For decreasing ambient temperature, an increasing effect of evaporative cooling is distinguishable as the pressure decreases until the moment that heat starts to be

released from the fuel. The reduced total pressure increase, and amount of evaporative cooling, is obvious from the 40-MPa cases by IFPEN, due to the lower mass-flow rate.

As with most of the ignition delay values shown in Fig. 4, Spray D tends to ignite slightly faster than Spray C. A very decent agreement in the initial pressure rise is found between results obtained at IFPEN and Sandia, shown in the insets of Fig. 5, and outliers appear rather random. For pressure-based ignition delay, variance in sensitivity of the sensors and the volumes naturally may influence the derived values to some extent, but this is expected to be constant for IFPEN and Sandia. However, an apparent discrepancy arises when comparing the ignition delay values of IFPEN at an injection pressure of 40 MPa. Based on the pressure-data, ignition delay values would range between 700 μs and 800 μs. Although this would correspond well with the trend shown by natural luminosity data by Caterpillar in Fig. 4, high-speed OH* data from IFPEN reveals values that are 100 to 200 μs shorter for Spray C and Spray D, respectively. Compared to the temperature variations with an injection pressure of 150 MPa, the total amount of fuel injected with injections of 40 MPa is reduced by approximately a factor of two [50]. Therefore, pressure increase during ignition, as well as the amount of light created in this process are influenced. For the chemiluminescence images, the intensity in the lift-off region is approximately a factor of two lower at the low injection pressure. Similarly, as mentioned before, the effect of evaporative cooling shown in the insets of Fig. 5 is much less pronounced due to the reduced mass flow, as is the pressure rise rate. As the optical ignition delay time values of the 40 MPa cases correspond to the inflection point of the pressure curves, the results are still expected to be correct. However, the sensitivity to the amount of fuel during ignition appears to be different depending on the ignition detection method.

Because of the uncertainties related to combustion indicators such as ignition delay and lift-off length for these larger sprays, new definitions should be investigated in future studies. Related to the greater volume in which ignition may take place, more of the chemiluminescence will be obscured by the spray along a line of sight. It is very well possible that the definitions are required to change with parametric variations to better align with the results from models. Furthermore, the parallax error for large differences in lift-off length values with parametric variations may need to be addressed. One approach to address some of the uncertainties is to study the effect of collection efficiency and working distances on combustion indicators in a single experimental setup.

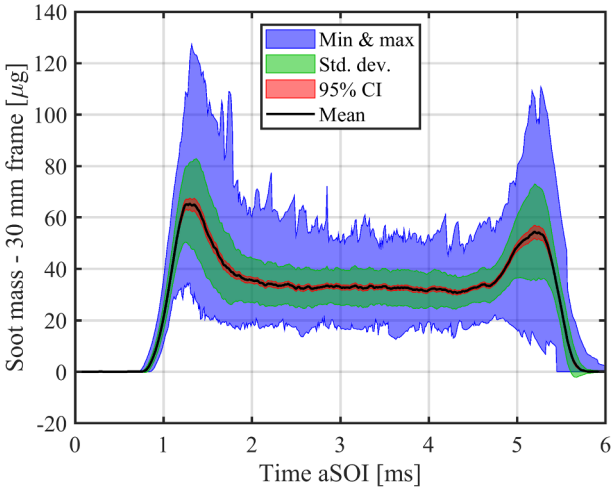


**Fig. 6.** Soot mass data from 200 Spray D experiments performed at Caterpillar, illustrating the variance of soot experiments under nominally identical boundary conditions. Soot mass is determined in a 30-mm window starting from the soot-inception point for this figure.

### 4.4. Soot emissions

Utilizing the high-repetition rate of the constant-flow facility at Caterpillar, 200 repetitions of soot extinction experiments for Spray D were conducted to better study the shot-to-shot variability of soot in sprays. Results are shown in Fig. 6, where soot mass is evaluated in a 30-mm interrogation window from the point where soot is first detected when moving downstream from the injector (note that a considerable part of these large sprays is outside the field-of-view of the DBI diagnostic). Considering the 95% confidence intervals around the mean, a high degree of convergence is achieved in the data-set for this number of experiments. However, from the minimum and maximum, it becomes evident that a 50% deviation from the mean is easily attainable. If a nominally identical spray can produce three times less soot than another spray using current fuel-injection equipment, understanding the variation between individual sprays holds the potential of significant improvement in emission levels. As soot production is dependent on all the phenomena and boundary conditions upstream of the soot-inception point (i.e., the location where soot is first found), a higher variability in soot mass is more likely compared to upstream parameters of interest such as the lift-off length. For instance, a 10% difference in flame lift-off length may correspond to a factor 2 change in soot mass for the well-studied Spray A case [32].

Other phenomena that can be extracted from this figure are the relatively high reproducibility during the very first phase of soot production, and the high-production rate during both the start of soot formation (between 1 and 2 ms aSOI), as well as the burn-out phase after the end of injection (between 4.5 and 5.5 ms aSOI). Such features are also recognizable in supplementary movies, available on the ECN website [52]. During the initial pre-mixed burn, more fuel is burnt at once in the head of the forming spray. This jet head structure subsequently contains a greater portion of sooting mixture in the field-of-view. After the end of injection, combustion recession takes place (see Ref. [69]) and the 30-mm window first moves upstream with the soot inception point, and at that time the represented soot mass increases again. Subsequently, the window moves downstream and eventually outside of the field of view while soot mass values come down and the spray burns out.

#### 4.4.1. Forced FOV approach

Most of the soot in the flames studied in combustion vessels utilized for this study is outside the field-of-view (FOV) due to the relatively large flames within limited volumes. To compare soot mass values between different extinction measurements, a forced FOV approach is used. For all fuel sprays, a region confined by the spreading angle of the spray, the location of soot onset, and a fixed probe volume is used. With a known soot onset location ($S_{onset}$), fixed volume ($V_{soot}$), and spreading angle ($\theta$), the height ($h$) of such a conical frustum can be determined by solving

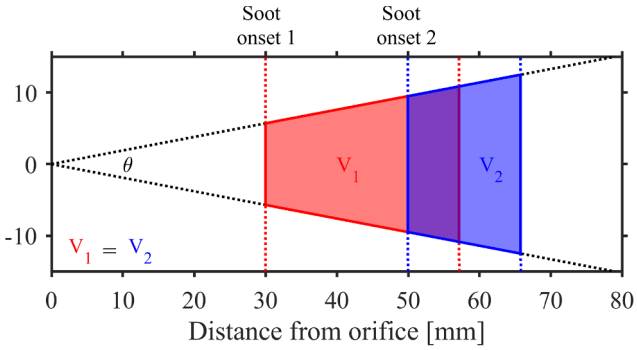


**Fig. 7.** Illustration of the approach used to investigate the soot mass in a region. The distance from the injector until which the mass is computed depends on the soot onset location, the spreading angle ($\theta$), and a pre-defined volume.

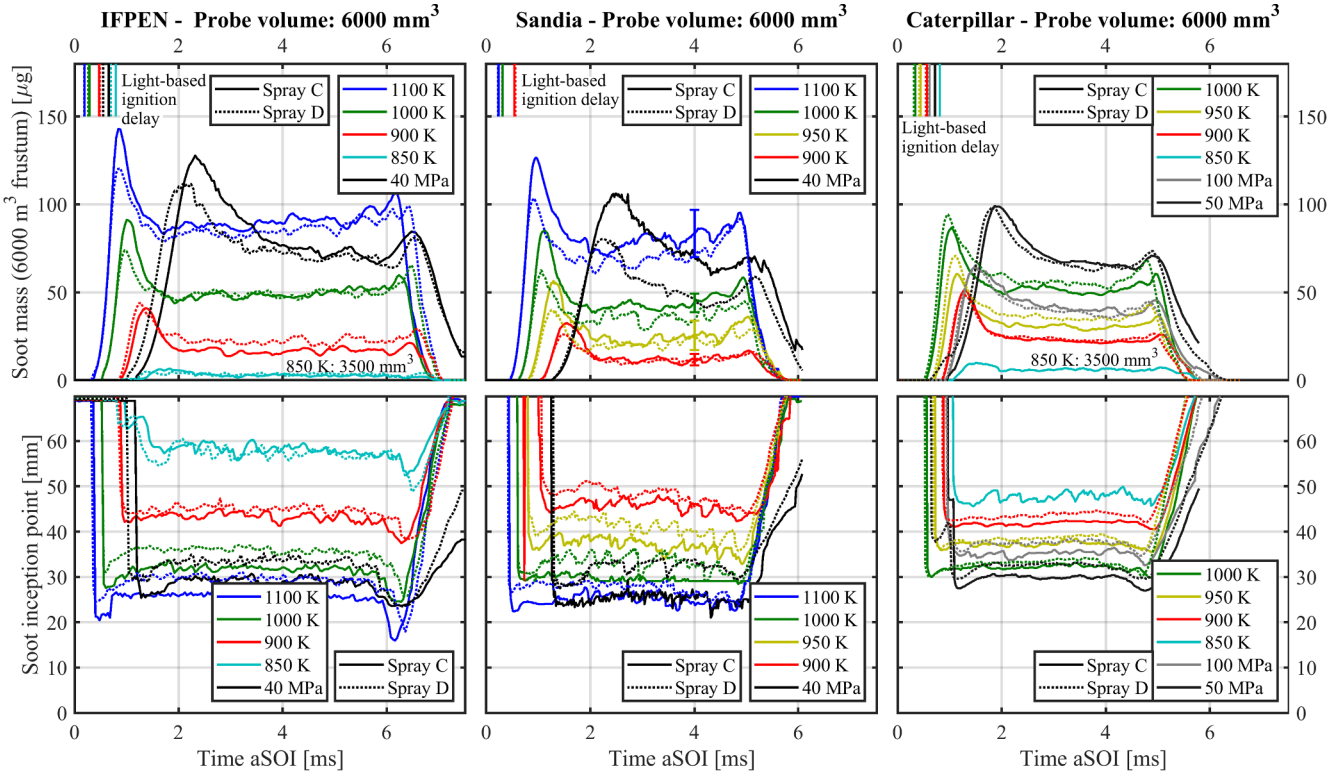


**Fig. 8.** Analysis of sooting behavior of the injectors as function of time in a probe volume of 6000 mm$^3$ starting from the soot inception point. The panels in the left column correspond to data obtained at IFPEN, the central column represents Sandia data, and the right column shows Caterpillar data. The top row panels represent the calculated soot mass in the pre-defined probe volume, and the bottom row panels show the soot inception point as distance from the injector orifice. The curves with different injection pressures correspond to an ambient temperature of 900 K. Error bars in the Sandia Spray C data at different temperatures indicate 95% confidence intervals using a t-distribution in the quasi-steady phase (at 4 ms).

$$h^3 + 3{\cdot}S_{onset}{\cdot}h^2 + 3{\cdot}S_{onset}^2{\cdot}h - \frac{3{\cdot}V_{soot}}{\pi{\cdot}tan^2(\theta/2)} = 0. \quad (7)$$

An example of this method is shown in Fig. 7. The figure shows two different cases which have a soot onset location of 30 mm and 50 mm from the injector orifice, respectively. The location until which the soot mass would be computed is shown with a second dashed line in the corresponding colors.

Despite the use of the volume to determine the investigated FOV, radial bounds are not respected in the actual computations. This is done to include turbulent vortices that shed soot particles outside the average spreading angle used in the computations. With the field-of-view in the IFPEN experiments extending to 67 mm, the soot onset location for the 900-K Spray D case was used to restrict the probe volume to 6000 mm$^3$ for comparing soot across the different conditions, which leaves a little room for fluctuations.

### 4.4.2. Soot mass results

Results from soot extinction measurements are shown in Fig. 8. The left column panels contain results obtained at IFPEN, and the middle and right columns represent data from Sandia and Caterpillar, respectively. The error bars in the Sandia results at 4 ms aSOI correspond to 95% confidence intervals using a t-distribution, similar to what is shown in Fig. 6. In this case, however, the confidence is reduced due to the decreased amount of experiments, and only shown at 4 ms to limit the amount of lines shown in this figure. Although not shown here, confidence intervals for IFPEN data are expected to be similar to the 900-K Spray C case by Sandia, which is based on 10 injections. For the 850-K cases at IFPEN, the probe volume of 6000 mm$^3$ was not achieved throughout the experiments, which is why a probe volume of 3500 mm$^3$ was used. Although the increased field-of-view in the Caterpillar experiments does allow the full volume to be attained for this ambient temperature, a similar probe volume was used to compare the data obtained at IFPEN and Caterpillar. The size of the volume is directly coupled to the soot inception point (via Eq. (7)), shown in the bottom row panels. For all variations in ambient temperature, results obtained at Sandia, Caterpillar and IFPEN are within a 20-$\mu$g proximity of each other during the quasi steady phase of the experiments, and therefore within the associated confidence intervals. For lower temperatures, the standard deviations and differences between institutions decrease. The locations of the peak soot mass and the first sign of soot, however, do reveal a slight time shift for each institution, which might be correlated to differences in light-based ignition delay from Fig. 4. The ignition delay values are indicated by vertical lines in the top-left corners of the soot mass panels. We discuss the relationship to soot inception and peak soot to ignition delay in more detail below.

With an exception of the cases that have an ambient temperatures of 1000 K and 1100 K, the spray head has left the field-of-view at the moment when the maximum soot mass of Fig. 8 is reached. Still, it is typically found that when the represented soot mass of either Spray C or Spray D is higher than the other in the spray head, this will persist into the quasi-steady phase. For all cases, the displayed soot mass is nearly the same for both injectors, when using the forced FOV approach with a fixed volume. At the most sooting conditions, Spray C produces higher amounts of soot for all the data shown. For IFPEN and Sandia data, Spray C starts to produce relatively less soot for decreasing temperatures compared to Spray D in the quasi-steady phase. This might be related to the equivalence ratio at the lift-off length, which will be treated in more detail further on. For Caterpillar such a trend is less obvious or not present at all, as displayed soot mass values are closer to one another in all cases. However, Spray D also produces relatively more soot when going from a 1000-K to a 950-K ambient.

Although within the confidence intervals when compared to IFPEN results, the Caterpillar data show higher soot values overall.

Presumably, the higher soot in this case is related to the different ambient composition. Note that there is still a 10-MPa injection pressure difference when comparing the lowest injection pressure cases, which will reduce the soot mass for the 50-MPa Caterpillar case with respect to results at 40 MPa. As identified in the section which describes the experimental facilities, the Caterpillar ambient does not contain any $CO_2$ or $H_2O$, whereas the IFPEN and Sandia vessels have around 6.5% and 3.7% of these constituents, respectively. Therefore, it is likely that the $CO_2$ and water content effectively reduces soot production in the IFPEN and Sandia experiments. In steady flames investigated at atmospheric pressure, the presence of water in the ambient gases reduced soot. This has been attributed to thermodynamics driving the reaction $OH + H_2 \rightleftharpoons H + H_2O$ in reverse leading to higher concentrations of the hydroxyl radical and enhanced soot precursor and soot oxidation [41]. This effect has been confirmed by recent experiments with representative high-temperature and high-pressure sprays from a 0.09-mm injector in a rapid compression machine, where both $CO_2$ as well as $H_2O$ dilution of the ambient gas resulted in reduced soot detection [45].

The location where soot is first detected shows a little more variation between different research institutes. The sprays into a 900-K ambient at Sandia consistently start to form soot further downstream than at IFPEN. For all other cases, the onset locations of IFPEN and Sandia are very alike, with Spray D showing the soot inception point downstream from that of Spray C. Although the latter holds for the Caterpillar results too, the difference between Spray C and Spray D is smaller, and soot onset locations for all cases appear closer to one another compared to IFPEN and Sandia. The Caterpillar data generally show soot inception closer to the injector, which is an expected result related to the ambient composition as discussed above. While it is generally clear that Spray C soot inception is upstream of Spray D, the lowest temperature case, 850 K at IFPEN, shows soot inception points that practically overlap.

The disadvantage of using a forced field-of-view approach to compare the soot mass for all different temperature variations and all research institutes is that most of the data is neglected, in order to accommodate the smallest windows, and cases with the least amount of soot. To investigate the effect of chosen volume on the measured soot mass, Fig. 9 shows the mean soot mass in the quasi-steady phase for data obtained in the Caterpillar facility. The Caterpillar data was chosen because trends can be observed up to twice the chosen volume because of the large field-of-view, cf. Table 1. The data is averaged between

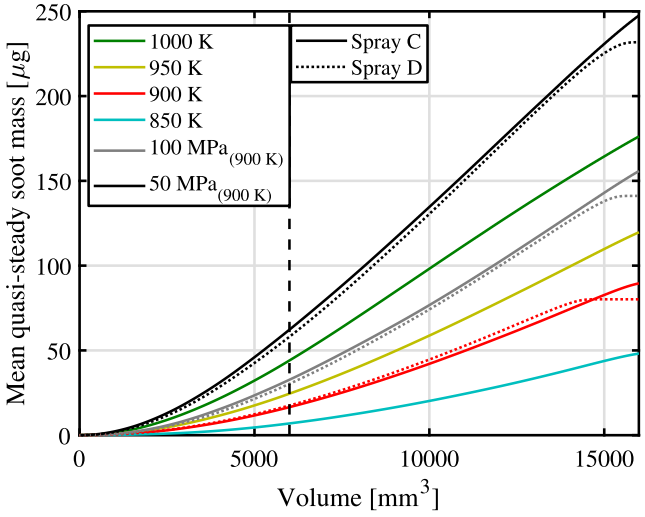


**Fig. 9.** Relationship between soot mass and probe volume that is investigated for different experiments performed at Caterpillar. For this comparison, the mean and ensemble-averaged quasi-steady soot mass is determined between 2500 and 4000 μs after the start of injection. The vertical dashed line indicates the 6000-mm$^3$ volume used for Fig. 7.

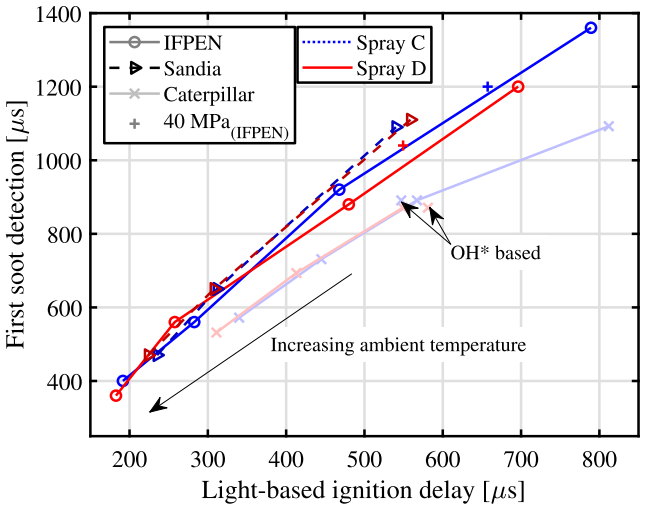


**Fig. 10.** Correlation between first soot detection and ignition delay for IFPEN, Sandia and Caterpillar. Light-based ignition delays by Caterpillar where derived from visible chemiluminescence movies, with exception of the indicated values at an ambient temperature of 900 K.

2500 and 4000 μs after the start of injection to capture the phase of the experiments where soot is not influenced by the start- or end of injection transients. The 6000-mm$^3$ value that was used for the profiles shown in Fig. 7 is indicated by the vertical dashed line. The leveling-off trends around the probe volume of 15000 mm$^3$ is caused by the fact that the end of the field-of-view is reached, at which point increasing the volume does not include more soot. More interesting than these effects, is how the relation between the mean quasi-steady soot mass is close to linear for most cases from the 6000-mm$^3$ volume all the way until the end of the FOV. When approaching the flame length, this trend is bound to discontinue, but it does provide a decent guideline to extrapolate the data over a significant portion of the spray for these relatively large sprays.

The sensitivity of soot inception to ignition delay can also be assessed by evaluating it against the time of first soot detection, which is shown based on a 1-μg threshold in Fig. 10. For all data shown, the observed trend is remarkably consistent between Spray C and Spray D experiments, as a slightly longer ignition delay retards the first soot detection. Moreover, the lines of IFPEN and Sandia show reasonable agreement over a large range of ignition delay times. However, the fact that both ignition delay and the moment of first soot detection is advanced for IFPEN data shows how it is likely that the Sandia ambient is less reactive.

As injection pressure affects temporal mixing (and not spatial mixing distribution) as long as cavitation effects are not altered, reducing injection pressure isolates entrainment effects [13]. Even when entrainment is lowered by reducing the injection pressure from 150 MPa to 40 MPa in IFPEN experiments, the points still fall on the same line, indicating how the difference in entrainment for these cases does not change that trend. However, this is not necessarily expected over a large range of parametric variations, as ignition delay and soot formation processes have different dependencies on the reactivity of the ambient, and equivalence ratio. As an example, the soot pyrolysis study by Skeen and Yasutomi [70], details conditions that result in significant divergence from the data shown in Fig. 10. For the low injection pressure case, the decrease in lift-off length results in a significantly higher equivalence ratio at the lift-off, and longer residence time for soot formation. This is because of an increase of the region in which high-temperature reactions take place, accompanied by reduced velocities. As a consequence a threefold increase in soot mass is observed in Fig. 8. In contrast to the overlap in IFPEN and Sandia data, the time of soot inception is clearly advanced for Caterpillar. Similar to the slightly

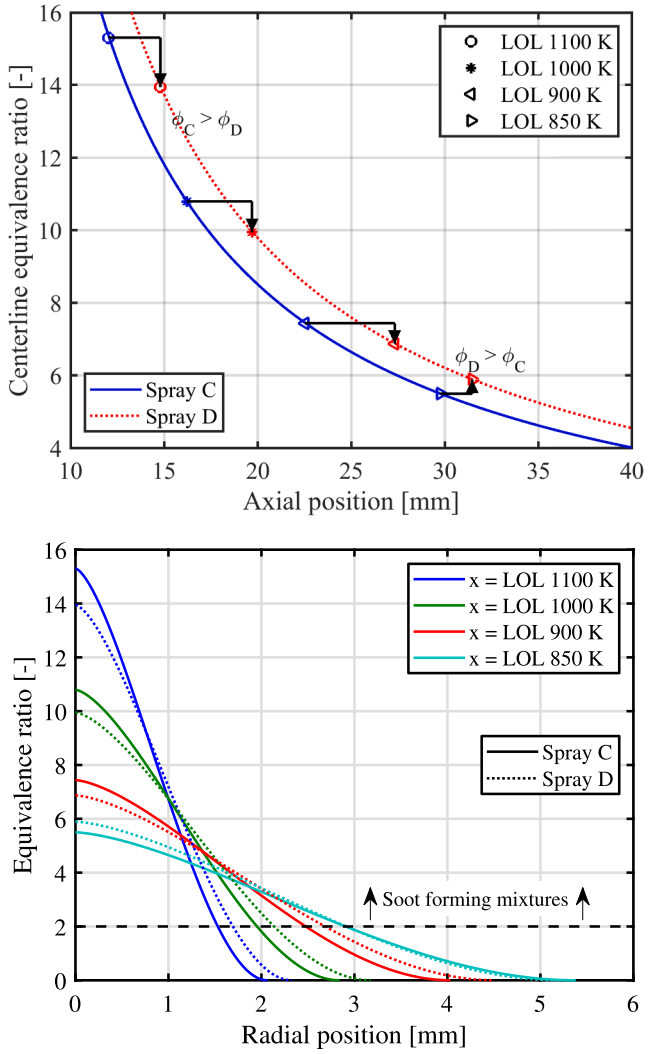


**Fig. 11.** Top: centerline equivalence ratio for Spray C and Spray D, illustrating how the lift-off region for spray D becomes more fuel-rich at lower temperatures. The black arrows identify these differences. Bottom: radial equivalence ratio distribution at the axial distance (x) that corresponds to the lift-off locations for both injectors with the sweep in ambient temperatures. Note that all lift-off values in this figure correspond to the IFPEN values.

increased soot mass, these results indicate how the lack of $CO_2$ and water presumably promotes soot production. The markers that do not fall on top of the lines are separate Caterpillar measurements of ignition delay using high-speed OH* chemiluminescence which were only obtained for the 900-K ambient temperature. The OH*-based measurements are scattered around that determined from the end-on view using visible-wavelength chemiluminescence, which provides confidence for the trustworthiness of the chemiluminescence thresholds used for the larger dataset.

### 4.5. Equivalence ratio predictions

To understand how the relative difference in soot mass and soot inception point for Spray C and Spray D experiments in Fig. 8 change as function of ambient temperature, predictions of mixing from the 1-D spray model described by Musculus and Kattke are used [47]. While Payri et al. showed decreased amounts of soot for a cylindrical nozzle in a different injector set [14], the model predictions are used to explain that this is caused by higher equivalence ratios at the lift-off length, as is the case in their study. The top panel of Fig. 11 shows the centerline equivalence ratio for the control volume at the lift-off length for both injectors, with the lift-off length values obtained at IFPEN identified by different markers as indicated in the legend. For the highest ambient temperature cases, the lift-off length of Spray C is shorter (horizontal axis), resulting in a relatively higher equivalence ratio at that axial distance (vertical axis). This difference is indicated using a black arrow. For the 850-K ambient, however, Spray D is more fuel rich at the lift-off length due to the reduced spreading angle. The mixture fraction model proposed by Siebers and modified by Musculus has been validated for relatively small fuel injector orifices (50, 71, 100, and 180 μm) [3]. In later work, area-average equivalence ratios were demonstrated to exhibit similarity to centerline equivalence ratios [13,47]. Since the orifices used in this work are even larger, the large radial width of the jets are expected to have a more significant impact on the location and timing of soot formation.

Variations of radial equivalence ratio profiles at the lift-off length are shown in the bottom panel of Fig. 11 for a range of ambient temperatures. The soot forming threshold for an equivalence ratio of two is denoted by a horizontal dashed line. As ambient temperature is reduced and lift-off length is extended, leaner centerline equivalence ratios are achieved and soot is reduced as a smaller volume of the jet exceeds the sooting threshold. The inversion of equivalence ratio, when reducing ambient temperatures, is visible in this panel too, particularly for rich, soot-forming mixtures at the jet centerline. However, Pickett and Siebers have shown how the soot inception point starts with a radial offset from the jet centerline when flames have a high sooting propensity, because of the reduced temperature local temperature [71]. Again, this indicates how not just the centerline equivalence ratio should be considered.

The radial fuel distribution difference between Spray C and Spray D predicted by the spray model at the lift-off length is evident from Fig. 11. As an alternative way to compare Spray C and Spray D, the total fuel mass available for soot formation was evaluated as well, reasoning that more fuel in rich combustion zones potentially leads to more soot. The fuel mass was determined in a volume bound by the lift-off length, and the end of the soot frustum used in Fig. 8. To limit the analysis to soot forming mixtures, only the part of that volume which exceeds the equivalence ratio of 2 is considered. Although Spray C is more fuel rich at the centerline, Spray D has on average 4.5% more fuel available in the fuel-rich volume discussed above, irrespective of the ambient temperature. Rather than comparing a similar volume one could asses the difference in sooting propensity by matching the fuel mass, which would increase the amount of soot mass from Spray C.

### 4.6. Soot results for short injections

As a second approach to compare Spray C and Spray D in terms of soot formation and oxidation, short injections with a net pressure increase of 35 kPa were targeted at Sandia. A 1200-K ambient was used to decrease the lift-off length and to reduce the burn-out duration. Three different injection pressures were selected to reduce the jet penetration such that the developing jet is nearly completely contained within the chamber for both soot formation and oxidation stages. Assuming that the combustion efficiency is equal for all cases, the 35 kPa pressure increase corresponds to a fixed amount of fuel with slightly different injection durations. This way, the effect of enhanced mixing by increasing injection pressure on the total soot mass can be evaluated in an isolated manner. The top panel of Fig. 12 shows the pressure increase for Spray C and Spray D in all considered cases, where the end of injection is indicated by representative line styles in the top of the panel. Despite not reaching the 35 kPa threshold within 2.5 ms, the cases with an injection pressure of 50 MPa eventually reach this value as well. The bottom panel of Fig. 12 illustrates how the total soot mass decreases in magnitude and burn-out duration with increasing injection pressure. The arrowheads in this panel indicate when the head of the jet reaches the end of the field-of-view. Evident from the movies and continuity of the displayed lines, is that the sprays have slowed down sufficiently by

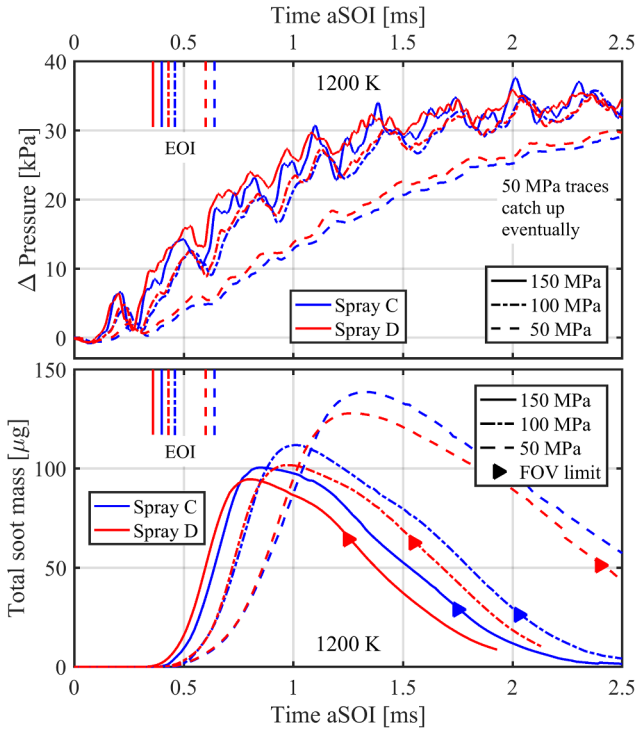


**Fig. 12.** Top: ensemble-averaged and filtered pressure increase for short injections into an 1200-K ambient at Sandia. All cases eventually reach 35 kPa. Bottom: total soot mass for short Spray C and Spray D injections at different injection pressures. The end of injection is also indicated for all cases in both panels. See text for more details.

this time, such that the effect of the spray leaving the field-of-view on the total soot mass is not even noticeable. Given that there is no reason to assume that combustion efficiency differs between these injectors, and that the pressure increase due to combustion is sufficiently close to warrant a comparison, we conclude that Spray C produces more soot at high ambient temperatures. That means that similar to the analysis before, enhanced mixing due to the increased spreading angle does not counterbalance the increased equivalence ratio at the lift-off length described in Fig. 11.

## 5. Summary and conclusions

In this work, nominally identical fuel injectors with orifice diameters on the order of 200 μm have been characterized at three different research institutes. The two different injectors considered in this work have minimal differences in mass flow and orifice diameter size; however, one of the injectors was manufactured with a straight hole and sharp orifice inlet to induce cavitation, while the other injector was subjected to hydro-erosive grinding and features a converging hole. From inert vapor penetration measurements at IFPEN and Sandia, it follows that the spray characteristics of the different injectors in two different combustion vessels are nearly identical.

When considering typical combustion indicators such as the lift-off length and the ignition delay, minor differences start to arise between the results obtained at different research institutes. While lift-off length values show decent agreement, ignition delay shows a rather ambiguous trend. Based on high-speed OH* experiments, IFPEN found shorter ignition delay times compared to Sandia and Caterpillar. This trend between IFPEN and Sandia, however, is not clearly observed when normalizing the pressure increase rate and extracting the ignition delay from a certain pressure threshold. The discrepancy in OH* derived ignition delays among the Sandia and IFPEN data is attributed to a small difference in the reactivity of the ambient. Considering that the observed differences in pressure-based ignition delays are mostly within the experimental uncertainty, it is assumed that further analysis of soot formation and consumption is still warranted.

Using a soot extinction imaging technique, the soot mass was quantified and compared for the Spray C and Spray D injectors across different combustion facilities. Observations in light-based ignition delay are shown to be reflected in the onset of soot formation based on these measurements. However, given the large variability of the amount of soot in a large set of data obtained in the Caterpillar combustion vessel, rather good agreement was found between the results of IFPEN, Sandia and Caterpillar across all ambient temperatures and injection pressures. In order to compare the results from these rather large sprays, a new approach that limits the field-of-view based on a fixed volume was used. Moreover, it was shown how the results from such a volume may be extrapolated downstream to simplify future comparisons. When comparing the constant pressure vessel of Caterpillar to the constant volume vessels of IFPEN and Sandia, an increased soot mass with a shorter soot inception time is found. In this work, it is rationalized how the $CO_2$ and water in the constant volume vessels (rather than just oxygen and nitrogen) reduce soot formation. In general, it is shown how Spray C produces more soot compared to Spray D, attributed to a higher equivalence ratio at the lift-off length. This was substantiated by short injection experiments conducted at Sandia, for which the total fuel energy was matched between injectors. However, when temperatures are reduced sufficiently, this trend appears to be reversed due to the different mixing behavior.

## CRediT authorship contribution statement

**Noud Maes:** Conceptualization, Data curation, Formal analysis, Investigation, Methodology, Validation, Visualization, Writing - original draft. **Scott A. Skeen:** Conceptualization, Data curation, Funding acquisition, Formal analysis, Investigation, Methodology, Validation, Visualization, Writing - review & editing. **Michele Bardi:** Conceptualization, Data curation, Formal analysis, Investigation, Methodology, Validation, Writing - review & editing. **Russell P. Fitzgerald:** Conceptualization, Data curation, Investigation, Methodology, Project administration, Funding acquisition, Writing - review & editing. **Louis-Marie Malbec:** Conceptualization, Formal analysis, Writing - review & editing. **Gilles Bruneaux:** Conceptualization, Project administration, Supervision, Funding acquisition, Writing - review & editing. **Lyle M. Pickett:** Conceptualization, Formal analysis, Investigation, Methodology, Project administration, Writing - review & editing. **Koji Yasutomi:** Conceptualization, Investigation, Writing - review & editing. **Glen Martin:** Conceptualization, Methodology, Data curation, Writing - review & editing.

## Declaration of Competing Interest

The authors declare that they have no known competing financial interests or personal relationships that could have appeared to influence the work reported in this paper.

## Acknowledgments

We thank Laurent Hermant for his technical assistance in the experiments conducted at IFPEN. The authors acknowledge the National Research Agency (contract ANR-14-CE22-0015-01) for financial support to the ECN-France project. Dr. Kenth I. Svensson is acknowledged for his valuable contributions to Caterpillar data and feedback. Experimental results presented by Sandia were conducted at the Combustion Research Facility, Sandia National Laboratories, Livermore, CA. Sandia research was sponsored by the U.S. Department of Energy (DOE) Office of Energy Efficiency and Renewable Energy (EERE) Vehicle Technologies Offices. Sandia National Laboratories is a

multi-mission laboratory managed and operated by National Technology and Engineering Solutions of Sandia, LLC., a wholly owned subsidiary of Honeywell International, Inc., for the U.S. Department of Energy's National Nuclear Security Administration under contract DE-NA0003525. Chris Carlen, Keith Penney, Aaron Czeszynski, and Dave Cicone are gratefully acknowledged for technical assistance. The authors also wish to thank Gurpreet Singh and Michael Weismiller, program managers at U.S. DOE, for their support.

## Appendix A. Supplementary material

Supplementary data associated with this article can be found, in the online version, at https://ecn.sandia.gov/pub-links/nm001/spraycd/.

## References

[1] I.A. Khalek, T.L. Bougher, P.M. Merritt, Phase 1 Of The Advanced Collaborative Emissions Study, SwRI Project No. 03.13062, 2009, pp. 1–158.
[2] H. Dwyer, A. Ayala, S. Zhang, J. Collins, et al., Emissions from a diesel car during regeneration of an active diesel particulate filter, J. Aerosol Sci. 41 (2010) 541–552.
[3] L.M. Pickett, D.L. Siebers, Non-Sooting, Low Flame Temperature Mixing-Controlled DI Diesel Combustion, SAE Technical Paper 2004-01-1399.
[4] R.K. Gehmlich, C.J. Mueller, D.J. Ruth, C.W. Nilsen, et al., Using ducted fuel injection to attenuate or prevent soot formation in mixing-controlled combustion strategies for engine applications, App. Energy 226 (2018) 1169–1186.
[5] M. Blessing, G. König, C. Krüger, U. Michels, et al., Analysis of Flow and Cavitation Phenomena in Diesel Injection Nozzles and Its Effects on Spray and Mixture Formation, SAE Technical Paper 2003-01-1358.
[6] R. Payri, J.M. García, F.J. Salvador, J. Gimeno, Using spray momentum flux measurements to understand the influence of diesel nozzle geometry on spray characteristics, Fuel 84 (2005) 551–561.
[7] F. Payri, J. Arrègle, J.J. López, S. Hermens, Effect of Cavitation on the Nozzle Outlet Flow, Spray and Flame Formation in a Diesel Engine, SAE Technical Paper 2006-01-1391.
[8] J.M. Desantes, R. Payri, F.J. Salvador, J. De la Morena, Influence of cavitation phenomenon on primary break-up and spray behavior at stationary conditions, Fuel 89 (2010) 3033–3041.
[9] S. Som, A.I. Ramirez, D.E. Longman, S.K. Aggarwal, Effect of nozzle orifice geometry on spray, combustion, and emission characteristics under diesel engine conditions, Fuel 90 (2011) 1267–1276.
[10] F.R. Westlye, M. Battistoni, S.A. Skeen, J. Manin, et al., Penetration and Combustion Characterization of Cavitating and Non-Cavitating Fuel Injectors under Diesel Engine Conditions, SAE Technical Paper 2016-01-0860.
[11] J.V. Pastor, J.M. García-Oliver, A. García, A.M. López, An Experimental Investigation on Spray Mixing and Combustion Characteristics for Spray C/D Nozzles in a Constant Pressure Vessel, SAE Technical Paper 2018-01-1783.
[12] L.M. Pickett, D.L. Siebers, C.A. Idicheria, Relationship Between Ignition Processes and the Lift-Off Length of Diesel Fuel Jets, SAE Technical Paper 2005-01-3843.
[13] L.M. Pickett, J. Manin, C.L. Genzale, D.L. Siebers, et al., Relationship between diesel fuel spray vapor penetration/dispersion and local fuel mixture fraction, SAE Int. J. Engines 2 (2011) 764–799.
[14] F. Payri, J. Lopez, A. Garcia, O. de la Garza de Leon, et al., Effects of Cavitation in Common-Rail Diesel Nozzles on the Soot Formation Process, SAE Technical Paper 2013-01-1602.
[15] J. Tang, S. Pischinger, M. Lamping, T. Körfer, M. Tatur, D. Tomazic, Coking phenomena in nozzle orifices of DI-diesel engines, SAE Int. J. Fuels Lubr. 2 (1) (2009) 259–272.
[16] O. Asi, Failure of a diesel engine injector nozzle by cavitation damage, Eng. Fail. Anal. 13 (2006) 1126–1133.
[17] M. Bardi, R. Payri, L.M. Malbec, G. Bruneaux, et al., Engine combustion network (ECN): comparison of spray development, vaporization, and combustion in different combustion vessels, Atomization Spray 22 (10) (2012) 807–842.
[18] M. Meijer, L.M.T. Somers, J. Johnson, J. Naber, et al., Engine combustion network (ECN): characterization and comparison of boundary conditions for different combustion vessels, Atomization Spray 22 (9) (2012) 777–806.
[19] N. Maes, M. Meijer, N. Dam, B. Somers, et al., Characterization of Spray A flame structure for parametric variations in ECN constant-volume vessels using chemiluminescence and laser-induced fluorescence, Combust. Flame 174 (2016) 138–151.
[20] W.T. Chung, P.C. Ma, M. Ihme, Examination of diesel spray combustion in supercritical ambient fluid using large-eddy simulations, Int. J. Engine Res. 21 (2020) 122–133.
[21] E.J. Pérez-Sánchez, J.M. Garcia-Oliver, R. Novella, J.M. Pastor, Understanding the diesel-like spray characteristics applying a flamelet-based combustion model and detailed large eddy simulations, Int. J. Engine Res. 21 (2020) 134–150.
[22] O.T. Kaario, V. Vuorinen, H. Kahila, H. Im, et al., The effect of fuel on high velocity evaporating fuel sprays: Large-Eddy simulation of Spray A with various fuels, Int. J. Engine Res. 21 (2020) 26–42.
[23] F. Tagliante, T. Poinsot, L.M. Pickett, P. Pepiot, et al., A conceptual model of the flame stabilization mechanisms for a lifted Diesel-type flame based on direct numerical simulation and experiments, Combust. Flame 201 (2019) 65–77.
[24] P.C. Ma, H. Wu, T. Jaravel, L. Bravo, et al., Large-eddy simulations of transcritical injection and auto-ignition using diffuse-interface method and finite-rate chemistry, Proc. Combust. Inst. 37 (2019) 3303–3310.
[25] P. Kundu, M. Ameen, C. Xu, U. Unnikrishnan, et al., Implementation of detailed chemistry mechanisms in engine simulations, ASME J. Eng. Gas Turbines Power 141 (1) (2019) 011026 (10 pages).
[26] T. Lucchini, D. Pontoni, G. D'Errico, B. Somers, Modeling diesel combustion with tabulated kinetics and different flame structure assumptions based on flamelet approach, Int. J. Engine Res. 21 (2020) 89–100.
[27] A. Krisman, E.R. Hawkes, J.H. Chen, A parametric study of ignition dynamics at ECN Spray A thermochemical conditions using 2D DNS, Proc. Combust. Inst. 37 (2019) 4787–4795.
[28] J. Pastor, R. Payri, J. García-Oliver, J. Nerva, Schlieren Measurements of the ECN-Spray A Penetration under Inert and Reacting Conditions, SAE Technical Paper 2012-01-0456.
[29] B. Higgins, D. Siebers, Measurement of the Flame Lift-Off Location on DI Diesel Sprays Using OH Chemiluminescence, SAE Technical Paper 2001-01-0918.
[30] F.R. Westlye, K. Penney, A. Ivarsson, L.M. Pickett, et al., Diffuse back-illumination setup for high temporally resolved extinction imaging, Appl. Opt. 56 (17) (2017) 5028–5038.
[31] J. Manin, L. Pickett, S. Skeen, Two-color diffused back-illumination imaging as a diagnostic for time-resolved soot measurements in reacting sprays, SAE Int. J. Engines 6 (2013) 1908–1921.
[32] M. Bardi, G. Bruneaux, L. Malbec, Study of ECN Injectors' Behavior Repeatability with Focus on Aging Effect and Soot Fluctuations, SAE Technical Paper 2016-01-0845.
[33] J.V. Pastor, J.M. García-Oliver, R. Novella, T. Xuan, Soot quantification of single-hole diesel sprays by means of extinction imaging, SAE Int. J. Engines 8 (2015) 2068–2077.
[34] S.A. Skeen, J. Manin, L.M. Pickett, E. Cenker, et al., A progress review on soot experiments and modeling in the engine combustion network (ECN), SAE Int. J. Engines 9 (2016) 883–898.
[35] R.A. Dobbins, C.M. Megaridis, Absorption and scattering of light by polydisperse aggregates, Appl. Opt. 30 (1991) 4747–4754.
[36] S. Skeen, K. Yasutomi, E. Cenker, B. Adamson, et al., Standardized optical constants for soot quantification in high-pressure sprays, SAE Int. J. Engines 11 (2018) 805–816.
[37] O. Angrill, H. Geitlinger, T. Streibel, R. Suntz, et al., Influence of exhaust gas recirculation on soot formation in diffussion flames, Proc. Combust. Inst. 28 (2000) 2643–2649.
[38] F. Liu, H. Guo, G.J. Smallwood, Ö.L. Gülder, The chemical effects of carbon dioxide as an additive in an ethylene diffusion flame: implications for soot and NO_x formation, Combust. Flame 125 (2001) 778–787.
[39] A. Katoh, M. Shinoda, K. Kitagawa, A.K. Gupta, Visualization of steam addition effect on OH distribution in a flame by isotope shift/planar laser-induced fluorescence (IS/PLIF) spectroscopy, ASME J. Eng. Gas Turbines Power 128 (2004) 8–12.
[40] H. Guo, G.J. Smallwood, A numerical study on the influence of $CO_2$ addition on soot formation in an ethylene/air diffusion flame, Combust. Sci. Technol. 180 (2008) 1695–1708.
[41] F. Liu, J.L. Consalvi, A. Fuentes, Effects of water vapor addition to the air stream on soot formation and flame properties in a laminar coflow ethylene/air diffusion flame, Combust. Flame 161 (2014) 1724–1734.
[42] P. Ni, X. Wang, Modeling the formation of NO_x and soot emissions in a diesel engine at different humidity, Int. J. Green Energy 9 (2012) 815–828.
[43] X. Li, Z. Xu, C. Guan, Z. Huang, Impact of exhaust gas recirculation (EGR) on soot reactivity from a diesel engine operating at high load, App. Therm. Eng. 68 (2014) 100–106.
[44] Y. Gallo, V.B. Malmborg, J. Simonsson, E. Svensson, et al., Investigation of late-cycle soot oxidation using laser extinction and in-cylinder gas sampling at varying inlet oxygen concentrations in diesel engines, Fuel 193 (2017) 308–314.
[45] C. Patel, C. Hespel, T.L. Nguyen, F. Foucher, et al., Effect of Exhaust Gas Recirculation composition on soot in ECN Spray A conditions, OGST (2020), in press.
[46] M.P.B. Musculus, J.E. Dec, D.R. Tree, D. Daly, et al., Effects of Water-Fuel Emulsions on Spray and Combustion Processes in a Heavy-Duty DI Diesel Engine, SAE Technical Paper 2002-01-2892.
[47] M.P.B. Musculus, K. Kattke, Entrainment waves in diesel jets, SAE Int. J. Engines 2 (1) (2009) 1170–1193.
[48] L.M. Pickett, D.L. Siebers, An investigation of diesel soot formation processes using micro-orifices, Proc. Combust. Inst. 29 (2002) 655–662.
[49] M. Bardi, G. Bruneaux, A. Nicolle, O. Colin, Experimental Methodology for the Understanding of Soot-Fuel Relationship in Diesel Combustion: Fuel Characterization and Surrogate Validation, SAE Technical Paper 2017-01-0721.
[50] R. Payri, J. Gimeno, J. Cuisano, J. Arco, Hydraulic characterization of diesel engine single-hole injectors, Fuel 180 (2016) 357–366.
[51] L.M. Pickett, available at https://www.ecn.sandia.gov.
[52] N. Maes, https://ecn.sandia.gov/pub-links/nm001/spraycd/.
[53] S.A. Skeen, J. Manin, L.M. Pickett, Simultaneous formaldehyde PLIF and high-speed schlieren imaging for ignition visualization in high-pressure spray flames, Proc. Combust. Inst. 35 (2015) 3167–3174.
[54] N. Maes, N. Dam, B. Somers T. Lucchini, et al., Heavy-Duty Diesel Engine Spray Combustion Processes: Experiments and Numerical Simulations, SAE Technical Paper 2018-01-1689.
[55] P. Lillo, L. Pickett, H. Persson, O. Andersson, et al., Diesel spray ignition detection and spatial/temporal correction, SAE Int. J. Engines 5 (2012) 1330–1346.
[56] N. Maes, P.C. Bakker, N. Dam, B. Somers, Transient flame development in a constant-volume vessel using a split-scheme injection strategy, SAE Int. J. Fuels Lubr.

10 (2017) 318–327.
[57] P. Laven, available at http://www.philiplaven.com/mieplot.htm.
[58] D. Siebers, Liquid-Phase Fuel Penetration in Diesel Sprays, SAE Technical Paper 980809.
[59] R. Payri, J.M. García-Olivier, M. Bardi, J. Manin, Fuel temperature influence on diesel sprays in inert and reacting conditions, App. Therm. Eng. 35 (2012) 185–195.
[60] L.M. Pickett, C.L. Genzale, G. Bruneaux, L. Malbec, et al., Comparison of Diesel Spray Combustion in Different High-Temperature, High-Pressure Facilities, SAE Technical Paper 2010-01-2106.
[61] D. Siebers, Scaling Liquid-Phase Fuel Penetration in Diesel Sprays Based on Mixing-Limited Vaporization, SAE Technical Paper 1999-01-0528.
[62] N. Maes, N. Dam, B. Somers, B. Lucchini, et al., Experimental and numerical analyses of liquid and spray penetration under heavy-duty diesel engine conditions, SAE Int. J. Fuels Lubr. 9 (1) (2016) 108–124.
[63] W.H. Nurick, Orifice cavitation and its effect on spray mixing, J. Fluids Eng. 98 (1976) 681–687.
[64] D. Han, M.G. Mungal, Direct measurement of entrainment in reacting/nonreacting turbulent jets, Combust. Flame 124 (2001) 370–386.
[65] L.M. Pickett, D.L. Siebers, Soot in diesel fuel jets: effects of ambient temperature, ambient density, and injection pressure, Combust. Flame 138 (2004) 114–135.
[66] J.M. García-Oliver, L.M. Malbec, H. Baya Toda, G. Bruneaux, A study on the interaction between local flow and flame structure for mixing-controlled Diesel sprays, Combust. Flame 179 (2017) 157–171.
[67] N. Maes, M. Hooglugt, N. Dam, B. Somers, et al., On the influence of wall distance and geometry for high-pressure n-dodecane spray flames in a constant-volume chamber, Int. J. Engine Res. (2019).
[68] L.M. Pickett, Low flame temperature limits for mixing-controlled Diesel combustion, Proc. Combust. Inst. 30 (2005) 2727–2735.
[69] B. Knox, C. Genzale, L. Pickett, J. Garcia-Oliver, et al., Combustion Recession after End of Injection in Diesel Sprays, SAE Technical Paper 2015-01-0797.
[70] S.A. Skeen, K. Yasutomi, Measuring the soot onset temperature in high-pressure n-dodecane spray pyrolysis, Combust. Flame 188 (2018) 483–487.
[71] L.M. Pickett, D.L. Siebers, Soot formation in diesel fuel jets near the lift-off length, Int. J. Engine Res. 7 (2006) 103–130.